Available online at www.sciencedirect.com
ScienceDirect
Journal of Solid State Chemistry 180 (2007) 571–576
JOURNAL OF SOLID STATE CHEMISTRY
www.elsevier.com/locate/jssc

# Structural change of layered perovskite $La_2Ti_2O_7$ at high pressures

F.X. Zhang[a], J. Lian[a], U. Becker[a], R.C. Ewing[b,*], L.M. Wang[c], Jingzhu Hu[d], S.K. Saxena[e]

[a]*Department of Geological Sciences, University of Michigan, Ann Arbor, MI 48109, USA*
[b]*Departments of Geological Sciences, Nuclear Engineering and Radiological Sciences, and Materials Science and Engineering, University of Michigan, Ann Arbor, MI 48109, USA*
[c]*Department of Nuclear Engineering and Radiological Sciences, Ann Arbor, MI 48105, USA*
[d]*X17C of NSLS, Cars, University of Chicago, Upton, NY 11793, USA*
[e]*CeSMEC, Florida International University, Miami, FL 33199, USA*

Received 11 October 2006; received in revised form 10 November 2006; accepted 12 November 2006
Available online 21 November 2006

**Abstract**

The perovskite-related layered structure of $La_2Ti_2O_7$ has been studied at pressures up to 30 GPa using synchrotron radiation powder X-ray diffraction (XRD) and Raman scattering. The XRD results indicate a pronounced anisotropy for the compressibility of the monoclinic unit cell. The ratio of the relative compressibilities along the [100], [010] and [001] directions is ~1:3:5. The greatest compressibility is along the [001] direction, perpendicular to the interlayer. A pressure-induced phase transition occurs at 16.7 GPa. Both Raman and XRD measurements reveal that the pressure-induced phase transition is reversible. The high-pressure phase has a close structural relation to the low-pressure monoclinic phase and the phase transition may be due to the tilting of $TiO_6$ octahedra at high pressures.


*Keywords:* $La_2Ti_2O_7$; High pressure; XRD; Raman; Phase transition

## 1. Introduction

Perovskite and materials with perovskite-related structures display a broad range of structural, chemical and physical properties [1–4]. Several compounds with the formula $A_2B_2O_7$, such as $La_2Ti_2O_7$, $Ca_2Nb_2O_7$, and $Nd_2Ti_2O_7$, do not form the expected isometric pyrochlore structure-type, as is typical for many of the heavy-rare earths and transition metal oxides, but rather form a layered structure comprised of slabs of the $ABO_3$ perovskite structure [5–7]. The layered perovskite $A_2B_2O_7$ belongs to the homologous series $A_nB_nO_{3n+2}$ with $n = 4$. Fig. 1 shows the schematic crystal structures of $La_2Ti_2O_7$ projected along the [100] and [010] directions, respectively. The perovskite "slab" contains four layers of corner-sharing $BO_6$ octahedra. The octahedra in different slabs are separated by two layers of *A*-site cations, La3 and La4. Lanthanum titanates in this homologous series exhibit a strong piezoelectric and electro-optic effect [1]. In addition, $La_2Ti_2O_7$ is ferroelectric with a high Curie temperature ($T_c = 1500\,^{\circ}C$) and has a high dielectric constant ($\varepsilon_r = 42$–$62$) with a low-temperature coefficient and a low dielectric loss at microwave frequency [8,9]. Recently, $La_2Ti_2O_7$ and other layered perovskites have received considerable attention because of their good photocatalytic activity in the water-splitting reaction, which has potential applications in fuel cell and other energy conversion technologies [10].

The room temperature structure of $La_2Ti_2O_7$ is monoclinic, $P2_1$ [6,11]. At ~780 °C, the structure becomes orthorhombic, $Cmc2_1$ [5] and at 1500 °C, it transforms into the paraelectric *Cmcm* phase. Resistivity measurements at low temperature for some of these layered perovskites along the *a*-, *b*- and *c*-axis, revealed a highly anisotropic conductivity [5,12], and they are quasi one-dimensional metals that display temperature-driven, metal–semiconductor transitions at lower temperatures.

*Corresponding author. Fax: +1 734 647 5706.
*E-mail address:* rodewing@umich.edu (R.C. Ewing).

0022-4596/$ - see front matter © 2006 Elsevier Inc. All rights reserved.
doi:10.1016/j.jssc.2006.11.022

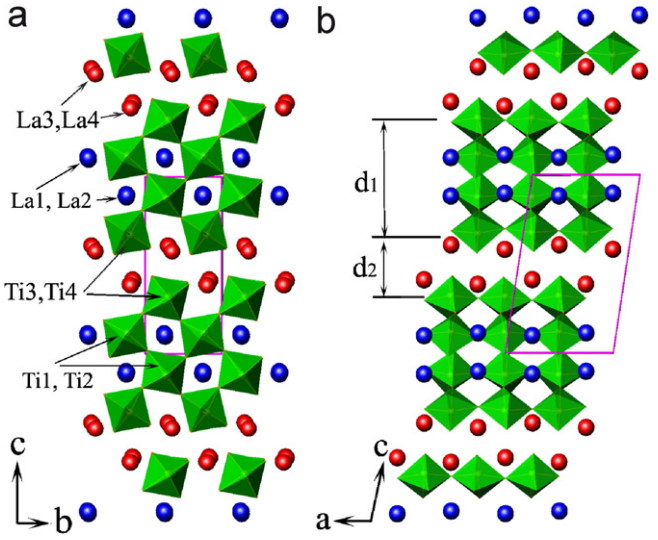


Fig. 1. The crystal structure of monoclinic $La_2Ti_2O_7$ can be represented by slabs of corner-sharing $TiO_6$ octahedra.

External pressure can be used to "tune" the structure and properties of materials. Pressure effects on $LaTiO_{3.41}$, which belongs to the $n = 5$ of the homologous series, have been recently studied [13] and unusually anisotropic compressibilities and a pressure-induced phase transition were reported. In this paper, we report the structural behavior of the monoclinic $La_2Ti_2O_7$ at pressures up to 30 GPa.

## 2. Experimental

$La_2Ti_2O_7$ perovskite was synthesized as a powder by a high temperature solid state reaction method. Pressure experiments were performed in a diamond anvil cell (DAC) using stainless steel gaskets for both the XRD and Raman measurements. Standard methanol/ethanol (4:1) liquid was used as pressure medium for all experiments. The in situ high-pressure XRD measurements were performed using a synchrotron radiation X-ray source with wavelength $\lambda = 0.4066$ Å and beam size of 35 μm at the 17C station of the National Synchrotron Light Source (NSLS) at Brookhaven National Laboratory. The Bragg diffraction rings were recorded with an image plate in transmission mode, and the XRD patterns were integrated from the images with FIT2d software [14]. The XRD patterns at low pressures were analyzed by a Rietveld-type refinement method using Fullprof [15]. Raman spectra were collected by using a high throughput holographic imaging spectrograph with volume transmission grating, holographic notch filter, and a thermoelectrically cooled charge coupled device (CCD) system (Physics Spectra). The light is 783.54 nm in wavelength from a He–Ne laser and the laser power was maintained below 5 mW to avoid heating of the sample. The pressure was measured by the ruby fluorescence method [16].

## 3. Results and discussion

The analysis of the powder X-ray diffraction patterns confirms a monoclinic structure for $La_2Ti_2O_7$ at ambient conditions. The refinement of the XRD pattern results in unit cell parameters of $a = 7.7775(4)$ Å, $b = 5.5248(3)$ Å, $c = 13.004(1)$ Å and $\beta = 98.58(2)^\circ$, which is in good agreement with literature values [10]. The evolution of the XRD patterns of $La_2Ti_2O_7$ with increasing pressure is shown in Fig. 2. The diffraction peaks in the patterns shift and broaden continuously until reaching a pressure of 16.7 GPa. At higher pressures, additional diffraction maxima appear in the pattern, which is the first indication of a pressure-induced phase transition that is completed at 30.2 GPa. The high-pressure phase has quite a different pattern from the low-pressure phase, especially for the relative intensities of some strong diffraction peaks. The diffraction pattern at 0.3 GPa, attained during unloading, however, is very close to the XRD pattern of the starting materials; thus, the pressure-induced phase transition is reversible. Because of its low symmetry, the diffraction peaks of the low-pressure phase display major overlaps at high pressures. The unit cell parameters were determined by Rietveld-type fits of the patterns, rather than indexing from the fitting of the individual

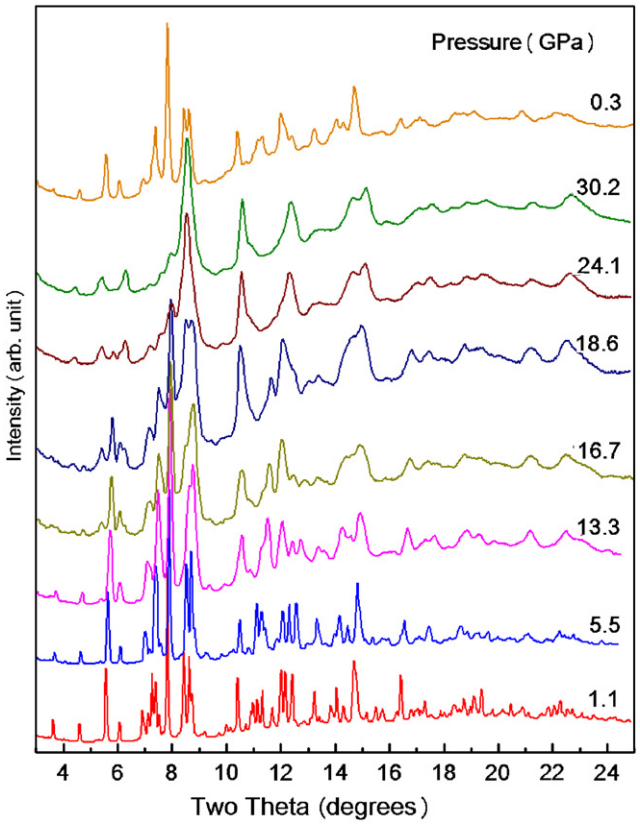


Fig. 2. The X-ray diffraction patterns of $La_2Ti_2O_7$ as a function of increasing pressure.

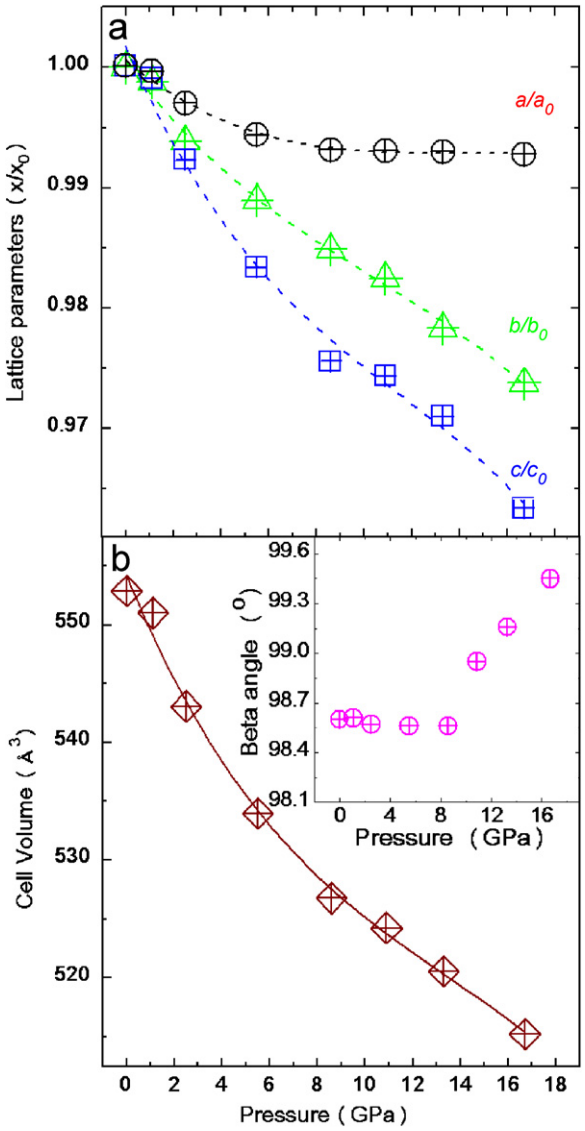


Fig. 3. Structural parameters of $La_2Ti_2O_7$ as a function of increasing pressure: (a) lattice parameters $a$, $b$ and $c$ normalized to the values at atmospheric pressure; (b) unit cell volume with increasing pressure. The inset shows the change in $\beta$ with increasing pressure. The solid line is the fit using the Murnaghan equation of state.

peaks. Fig. 3a shows the change in the relative values of the unit cell parameters with increasing pressure for monoclinic $La_2Ti_2O_7$. The compressibility is quite anisotropic, and the compressibility along the long $c$-axis shows the largest value. The relative compressibilities along the $a$-, $b$- and $c$-axis have an approximate ratio of 1:3:5. The $a$-axis is along a line formed by the opposite apices of the corner-sharing $TiO_6$ octahedra, and the structure can respond by the pressure-induced compression of the $TiO_6$ octahedra. The $b$-axis is nearly parallel to the edges of the $TiO_6$ octahedra, and increasing pressure causes a tilting of the $TiO_6$ octahedra (Fig. 1a), which makes this material softer in the $b$ compared with the $a$ direction. The monoclinic $\beta$-angle does not change significantly at pressures below 8.6 GPa. At higher pressures, it increases gradually (inset in Fig. 3b). The change in cell volume with increasing pressure is shown in Fig. 3b. The experimental data can be represented by a Murnaghan equation [17] $V(P) = V_0[(B'/B_0)P + 1]^{-1/B'}$ with bulk modulus $B_0 = 121(23)$ GPa, the pressure derivation of the bulk modulus at zero pressure $B' = 18(5)$, and an ambient pressure cell volume of 525.5(2) $Å^3$. The calculated bulk modulus of $La_2Ti_2O_7$ is slightly less than that of $LaTiO_{3.41}$ (142 GPa) [13].

The pressure dependent curves of the lattice parameters $a$, $c$ and the $\beta$ angle of the monoclinic $La_2Ti_2O_7$ in Fig. 3 show bending at pressure of 8.6 GPa. It indicates that some structural stability may happen at this pressure. From the measured XRD patterns, however, it is difficult to state that the above change is caused by any structural transformation.

There are 4 La ions, 4 Ti ions and 14 O anions in the unit cell, and they all occupy the 2$a$ Wyckoff positions. Thus, it is impossible to make full Rietveld refinement of all of the atomic coordinates at high pressures. However, a Rietveld-type fit was performed by just accounting for the variation of heavy atoms, La and Ti, in the unit cell; thus, all of the structural information can be obtained, except the oxygen positions in the $TiO_6$ octahedra. The thickness of the four layers of $TiO_6$ octahedral slab, $d_1$, and the interlayer separation of the slabs, $d_2$, can be estimated from the $z$-coordinates of Ti3 and Ti4. The complicated changes of the $z$-coordinates of Ti3 and Ti4 with pressure are plotted in Fig. 4a, and their average value reveals a gradual increase with increasing pressure. The slab thickness is only determined by the average of the $z$-coordinates of Ti3 and Ti4. In fact, under ambient conditions, Ti3 and Ti4 atoms are nearly in the same plane, and the calculated slab thickness is $d_{10} = 8.31$ Å, and the interlayer separation is $d_{20} = 4.55$ Å. The relative slab thickness $d_1/d_{10}$ and interlayer separation $d_2/d_{20}$ at high pressures, estimated from the average value of the $z$-coordinates of Ti3 and Ti4, are plotted in Fig. 4b. This shows that the large compressibility along the $c$-axis is mainly due to the compression of theinterlayer.

The interlayer separation can also be estimated from the $z$-coordinates of the rare earth ions, La3 and La4. From the Rietveld-type fitting of the XRD patterns, the evolution of the $y$ and $z$ coordinates of La3 and La4 with pressure is shown in Fig. 5. The $y$ coordinate of La3 and La4 has a complicated behavior of change with pressure, while the $z$-coordinate of both ions shows little change with increasing pressure, and their average value is nearly pressure independent.

For the high-pressure phase, it is difficult to obtain any structural details from the XRD patterns. The phase transition is complete at 30.2 GPa; however, some of the strong diffraction peaks of the monoclinic phase still show some intensity, which indicates that the high-pressure phase has a close structural relation to the low-pressure

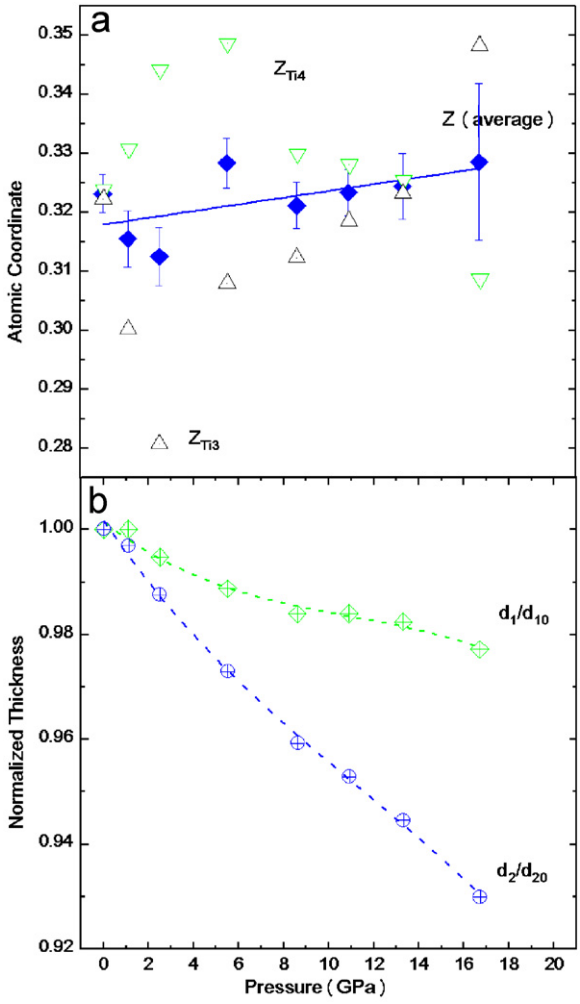


Fig. 4. (a) Refined $z$-coordinates of Ti3 and Ti4 at various pressures, the solid line is their average values. (b) Pressure dependence of the calculated relative slab thickness, $d1$, and the interlayer separation, $d2$, normalized to ambient pressure values.

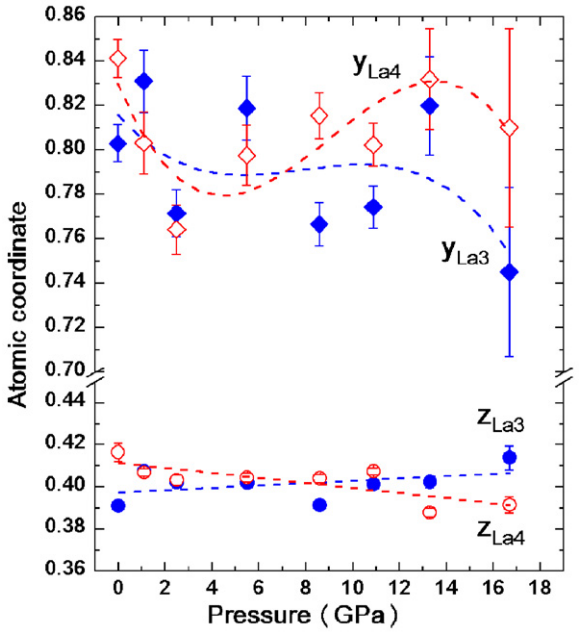


Fig. 5. The $y$ and $z$ coordinates of atoms La3 and La4 refined from the XRD patterns at various pressures. The dashed lines are not quantitative fits, but as for a visual estimate.

Table 1
Indexing results of the high-pressure phase at 30.2 GPa

| $h\,k\,l$ | $d_{obs}$ (Å) | $d_{cal}$ (Å) | $\delta d$ (Å) | $I/I_0$ |
|---|---|---|---|---|
| 0 1 0 | 5.232 | 5.229 | 0.003 | 7 |
| 1 1 0 | 4.310 | 4.328 | −0.019 | 15 |
| 0 1 2 | 3.987 | 3.995 | −0.008 | 6 |
| 1 1 −2 | 3.694 | 3.709 | −0.015 | 18 |
| 0 1 −3 | 3.246 | 3.240 | 0.006 | 6 |
| −2 0 3 | 3.070 | 3.078 | −0.008 | 12 |
| −2 1 2 | 2.934 | 2.932 | 0.002 | 25 |
| 1 0 4 | 2.726 | 2.725 | 0.001 | 100 |
| 3 0 −3 | 2.363 | 2.361 | 0.002 | 3 |
| 0 2 3 | 2.205 | 2.209 | −0.004 | 34 |
| 1 2 4 | 1.887 | 1.886 | 0.001 | 28 |
| −1 3 3 | 1.595 | 1.592 | 0.002 | 21 |
| 5 0 0 | 1.544 | 1.543 | 0.001 | 27 |
| −2 0 9 | 1.368 | 1.368 | −0.000 | 8 |
| 0 3 6 | 1.331 | 1.332 | −0.001 | 9 |
| −4 1 8 | 1.276 | 1.276 | 0.000 | 4 |
| 4 3 2 | 1.239 | 1.239 | 0.000 | 5 |
| −5 2 6 | 1.196 | 1.196 | 0.000 | 6 |
| 2 1 10 | 1.102 | 1.102 | 0.000 | 6 |
| 6 2 4 | 1.033 | 1.033 | −0.000 | 11 |

Unit cell parameters: $a = 7.819(4)$ Å, $b = 5.239(3)$ Å, $c = 12.550(6)$ Å, and $\beta = 99.33(4)^\circ$.

monoclinic phase. The structural transition is probably due to the pressure-induced tilting of the $TiO_6$ octahedra. There are two polymorphs with orthorhombic structures for $La_2Ti_2O_7$ at high temperatures, and the XRD pattern of the high pressure phase is obviously not the orthorhombic phase. Though there is massive overlap for the diffrac tion peaks, indexing of all of the peaks at 30.2 GPa results in a monoclinic unit cell with lattice parameters of $a = 7.819(4)$ Å, $b = 5.239(3)$ Å, $c = 12.550(6)$ Å, and $\beta = 99.33(4)^\circ$. The calculated and observed $d$-values of the high-pressure phase are listed in Table 1. Due to the low symmetry, every diffraction peak may, in fact, correspond to several peaks with different Miller indexes. The indexed lattice parameters are quite close to those of the low-pressure phase. The lattice parameter $a$ is a little larger than that of the starting material at atmospheric pressure. This may be caused by the deviation during calculation. The lattice parameters of the low-pressure phase are derived from the Rietveld-like refinement of the whole diffraction pattern, while the lattice parameters for the high-pressure phase are calculated from the indexing of the individual diffraction peaks. The massive overlapping of the diffraction peaks at high pressures may lead to a larger deviation of the lattice parameters. However, the

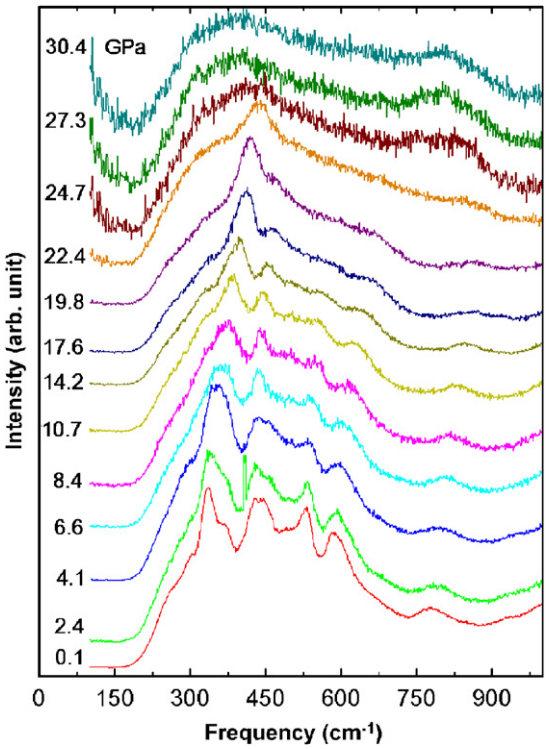


Fig. 6. The evolution of Raman spectrum of $La_2Ti_2O_7$ with increasing pressure.

calculated unit cell volume of the high-pressure phase at 30.2 GPa is 507.3 $Å^3$, which is in good agreement with the tendency of the $P$–$V$ curve of the low pressure phase shown in Fig. 3b. The similarities of the lattice parameters of the low- and high-pressure phases of $La_2Ti_2O_7$ suggest that the pressure-induced phase transition may be only due to a symmetry change. The first peak indexed as (010) in Table 1 suggests that the space group of the high-pressure phase can only be $P2$ (No.3), $Pm$ (No.6) or $P2/m$ (No.10). Another possibility is that the symmetry of the high-pressure phase is the same as the low-pressure phase, but the $b$ parameter of the indexed unit cell of the high-pressure phase is doubled. For the latter case, the high-pressure phase is just a superstructure of the low-pressure phase. With the present XRD data, it is not possible to derive further structural information about the high-pressure phase from the XRD patterns due to the significant overlapping of the diffraction peaks.

The Raman spectra of $La_2Ti_2O_7$ were measured at pressures up to 30 GPa. Fig. 6 shows the evolution of the observed Raman spectra with increasing pressure at frequencies below 1000 $cm^{-1}$. The $La_2Ti_2O_7$ is monoclinic ($P2_1$) and all 22 atoms occupy the $2a$ positions in the unit cell. Similar to the XRD patterns, the Raman spectrum also has major overlaps of the modes because the symmetry allows 132 Raman-active modes. The measured spectrum is in general agreement with that previously observed [18]. The intensity of the observed bands decreases with increasing pressure. The positions of all the bands change continuously with pressure, and they all lose their intensity above 25 GPa. The continuous change of the Raman bands also indicates that the pressure-induced phase transition is a continuous rather than a reconstructive transition, which is in agreement with the interpretation of the XRD data.

## 4. Conclusions

The structural evolution of layered perovskite structure of $La_2Ti_2O_7$ was determined at pressures up to 30.2 GPa. The compressibility of the unit cell is highly anisotropic. The ratio of the compressibilities along the $a$-, $b$- and $c$-axis is about 1:3:5, and the interlayer separations (perpendicular to the $c$-axis) are greatly compressed at high pressures. A pressure-induced reversible phase transition is observed at pressures above 16.7 GPa, and the high-pressure phase is a result of a continuous change in the low-pressure phase. The pressure-induced tilting of the $TiO_6$ octahedra may result in a change of symmetry or the formation of a supercell.

## Acknowledgments

This work was support by the Office of Basic Energy Sciences of the US Department of Energy, through Grant no. DE-FG02-97ER45656 and the NSF NIRT program (EAR-048563). The Raman measurements performed in CESMEC, FIU, were financially supported by Grants from the National Science Foundation (DMR-0231291, EAR-00769641). The use of the National Synchrotron Light Source at 17C station is supported by NSF COMPRES EAR01-35554 and by US-DOE contract DE-AC02-10886.

## References

[1] F. Lichtenberg, A. Herrnberger, K. Wiedenmann, J. Mannhart, Prog. Solid State Chem. 29 (2001) 1.
[2] T. Willams, H. Schmalle, A. Reller, F. Lichtenberg, D. Widmer, G. Bednorz, J. Solid State Chem. 93 (1991) 534.
[3] P.A. Fuierer, R.E. Newnham, J. Am. Ceram. Soc. 74 (1991) 2876.
[4] A. Ohtomo, D.A. Muller, J.L. Grazul, H.Y. Hwang, Appl. Phys. Lett. 80 (2002) 3922.
[5] N. Ishizawa, F. Marumo, S. Iwai, M. Kimura, T. Kawamura, Acta Crystallogr. B 38 (1982) 368.
[6] N. Ishizawa, F. Marumo, S. Iwai, M. Kimura, T. Kawamura, Acta Crystallogr. B 36 (1980) 763.
[7] M. Kimura, S. Nanamatsu, T. Kawamura, S. Matsushita, Jpn. J. Appl. Phys. 13 (1974) 1473.
[8] S. Nanamatsu, M. Kimura, J. Phys. Soc. Jpn. 36 (1974) 1495.
[9] S. Nanamatsu, M. Kimura, K. Doi, S. Matsushita, N. Yamada, Ferroelectrics 8 (1974) 511.
[10] D.W. Huang, J.S. Lee, W. Li, S.H. Oh, J. Phys. Chem. B 107 (2003) 4963.
[11] P.M. Gasperin, Acta Crystallogr. B 31 (1975) 2129.
[12] C.A. Kuntscher, D. van der Marel, M. Dressel, F. Lichtenberg, J. Mannhart, Phys. Rev. B 67 (2003) 035105.

[13] I. Loa, K. Syassen, X. Wang, F. Lichtenberg, M. Hanfland, C.A. Kuntscher, Phys. Rev. B 69 (2004) 224105.
[14] A. Hammersley, Computer Program Fit 2d, ESRF, Grenoble, 1998.
[15] T. Roisnel, J. Rodriguez-Carvajal, Material Science Forum, Proceedings of the 7th European Powder Diffraction Conference (EPDIC7), vol. 118, 2000.
[16] H.K. Mao, J. Xu, P.M. Bell, J. Geophys. Res. 91 (1986) 4673.
[17] F.D. Murnaghan, Proc. Natl. Acad. Sci. USA 30 (1944) 244.
[18] J. Takahashi, T. Ohtsuka, J. Am. Ceram. Soc. 72 (1989) 426.